Mdm1/Snx13 is a novel ER–endolysosomal interorganelle tethering protein

W. Mike Henne,[1] Lu Zhu,[2,3] Zsolt Balogi,[2,3] Christopher Stefan,[4] Jeffrey A. Pleiss,[2] and Scott D. Emr[2,3]

[1]Department of Cell Biology, University of Texas Southwestern Medical Center, Dallas, TX 75390
[2]Department of Molecular Biology and Genetics and [3]Weill Institute for Cell and Molecular Biology, Cornell University, Ithaca, NY 14853
[4]Medical Research Council Laboratory for Molecular Cell Biology, University College London, London WC1E 6BT, England, UK

Although endolysosomal trafficking is well defined, how it is regulated and coordinates with cellular metabolism is unclear. To identify genes governing endolysosomal dynamics, we conducted a global fluorescence-based screen to reveal endomembrane effector genes. Screening implicated Phox (PX) domain–containing protein Mdm1 in endomembrane dynamics. Surprisingly, we demonstrate that Mdm1 is a novel interorganelle tethering protein that localizes to endoplasmic reticulum (ER)–vacuole/lysosome membrane contact sites (MCSs). We show that Mdm1 is ER anchored and contacts the vacuole surface in trans via its lipid-binding PX domain. Strikingly, overexpression of Mdm1 induced ER–vacuole hypertethering, underscoring its role as an interorganelle tether. We also show that Mdm1 and its paralogue Ydr179w-a (named Nvj3 in this study) localize to ER–vacuole MCSs independently of established tether Nvj1. Finally, we find that Mdm1 truncations analogous to neurological disease–associated *SNX14* alleles fail to tether the ER and vacuole and perturb sphingolipid metabolism. Our work suggests that human Mdm1 homologues may play previously unappreciated roles in interorganelle communication and lipid metabolism.

Introduction

Endocytosis and the sorting of vesicles to lysosomes (vacuoles in yeast) is the major pathway by which transmembrane proteins are down-regulated. Genetic screens have identified machinery that mediates endolysosomal sorting, but how this machinery is regulated and coordinates with other cellular pathways is unclear. Identifying and characterizing these regulatory elements, as well as how endomembrane trafficking integrates into general cellular physiology, remain a major objective of the membrane trafficking field.

Previous studies revealed that endolysosomal trafficking is intimately related to interorganelle communication and lipid flux. The plasma membrane (PM) has a well-defined lipid composition that must be continually maintained to promote endocytic uptake (Munn et al., 1999). Sterols are particularly important for PM integrity, and loss of the sterol carrier oxysterol homology proteins leads to defects in endocytosis (Beh and Rine, 2004). Consistent with this, loss of proteins required for sterol biogenesis (*erg2*) and homeostasis (*arv1*) affect endocytosis (Beh and Rine, 2004). Sphingolipids are also essential to PM integrity and coassemble with sterols at the PM and endosomes, promoting endosomal maturation (Pichler and Riezman, 2004; Guan et al., 2009).

Further highlighting the connections between endomembrane trafficking and lipid metabolism is the recent observation that vesicle trafficking proteins may mediate interorganelle tethering. Two studies identified Vam6/Vps39, a component of the HOPS (homotypic fusion and vacuole protein sorting) vacuolar fusion complex, as a mediator of mitochondria–vacuole tethering. They further suggest that mitochondria–vacuole membrane contact sites (MCSs) are regions of phospholipid exchange, which, together with ER–mitochondrial encounter structures, are essential for mitochondrial lipid metabolism (Elbaz-Alon et al., 2014; Hönscher et al., 2014).

In addition to mitochondria, the ER also forms MCSs with endosomes and lysosomes (vacuoles in yeast; Pan et al., 2000; Eden et al., 2010; Friedman et al., 2013; Rowland et al., 2014). Indeed, EM studies showed that the ER and endosomes are closely juxtaposed, allowing the ER-resident phosphatase PTP1B to regulate the sorting of EGF receptors at late endosomes in trans (Eden et al., 2010). Additionally, the endosomal sterol-binding protein STARD3 has recently been proposed to bind in trans to ER-localized vesicle-associated proteins, thereby localizing sterol transfer to ER–endosome MCSs (Alpy et al., 2013). However, the machinery that establishes ER–en-

Correspondence to W. Mike Henne: Mike.Henne@utsouthwestern.edu; or Scott D. Emr: sde26@cornell.edu

Abbreviations used in this paper: CMAC, 7-amino-4-chloromethylcoumarin; DIC, dynamic interference contrast; FL, full length; GPD, glyceraldehyde 3-phosphate; KO, knockout; MCS, membrane contact site; nER, nuclear ER; NVJ, nER–vacuole junction; PM, plasma membrane; PMN, piecemeal autophagy of the nucleus; PX, Phox; PXA, PX associated; RGS, regulator of G protein signaling; SGA, synthetic genetic array; TEM, transmission EM.

The Rockefeller University Press $30.00
J. Cell Biol. Vol. 210 No. 4 541–551
www.jcb.org/cgi/doi/10.1083/jcb.201503088

dosome/lysosome MCSs in mammals is currently not defined and constitutes a major question in the understanding of ER–endolysosomal interorganelle communication.

Using synthetic genetic array (SGA) methodology and screening, we identify mitochondrial distribution and morphology 1 (Mdm1) as a protein required for the efficient vacuolar sorting of the endocytic reporter Mup1-pHluorin. Surprisingly, we find that Mdm1 is a novel ER–vacuole/lysosome MCS tethering protein that localizes specifically to nuclear ER (nER)–vacuole junctions (NVJs). Previously misannotated as a small soluble protein, we demonstrate that Mdm1 is an ER-anchored transmembrane protein that binds the vacuole in trans via its C-terminal Phox (PX) homology domain. We also characterize a novel Mdm1 paralogue Ydr179w-a, which we name Nvj3, and show that both it and Mdm1 localize specifically to NVJs in an Nvj1-independent manner. Remarkably, overexpression of Mdm1 hypertethers the nER to the vacuole. We also demonstrate that Mdm1 is a substrate for Nvj1-mediated piecemeal autophagy of the nucleus (PMN).

Unlike other yeast NVJ-resident proteins, Mdm1 is highly conserved in mammals as four sorting nexins (Snx): Snx13, 14, 19, and 25. Snx14 alleles are implicated in an autosomal-recessive neurological disease characterized by cellular vacuolization and granular plaque accumulation in late endosomes or autophagosomes (Thomas et al., 2014). We show that Snx14 disease-analogous mutations in Mdm1 fail to tether the ER and vacuole in yeast. Finally, we link Mdm1 proteins to lipid metabolism by showing that these disease-associated alleles induce hypersensitivity to the sphingolipid synthesis inhibitor myriocin. The identification of a highly conserved family of ER–endolysosomal tethering proteins in yeast opens the door for further mechanistic work characterizing the roles of ER–endosome/lysosome MCSs in endomembrane trafficking, lipid metabolism, and potentially, human neurological disease.

Results and discussion

A global membrane trafficking screen implicates PX domain–containing protein Mdm1 in endolysosomal dynamics

To uncover novel endolysosomal effector genes, we developed a fluorescence screen based on using the well characterized endocytic cargo Mup1 (Lin et al., 2008; Prosser et al., 2010; Henne et al., 2012; Buchkovich et al., 2013). Mup1 is the yeast methionine permease and localizes to the PM in yeast cultured without methionine. Upon methionine addition, Mup1 is ubiquitinated and sorted to the vacuolar lumen in an Art1 adaptor–dependent manner (Lin et al., 2008). To monitor Mup1 sorting, we conjugated it to the pH-sensitive GFP variant, pHluorin (Mup1-pH). Mup1-pH offers several advantages as a fluorescent endocytic reporter because it is abundant, its endocytosis is inducible, and it allows the differentiation between vacuolar sorted (quenched) versus nonsorted (fluorescent) pHluorin (Fig. 1 A).

Using SGA methodology (Costanzo and Boone, 2009), we introduced chromosomally tagged Mup1-pH into the yeast nonessential knockout (KO) collection, generating ∼4,700 unique haploid strains encoding *MUP1-PHLUORIN*. To assess each strain's ability to sort Mup1-pH, we used a two-stage screening strategy (Fig. 1 B). In the first stage, we used high-content flow cytometry, evaluating the fluorescence of thousands of yeast per strain. In a secondary screen, strains exhibiting significant fluorescence were imaged to confirm Mup1-pH sorting defects. From this screening, four classes of mutants were identified (Fig. 1 B).

Global Mup1-pH screening identified many known and uncharacterized ORFs whose deletions affect Mup1-pH sorting, and these will be more thoroughly analyzed in a subsequent study. In addition to many established membrane trafficking factors, screening implicated numerous lipid metabolism genes in Mup1 sorting, consistent with previous endomembrane trafficking screens (Fig. 1 C). Because we were most interested in endolysosomal dynamics, we conducted a tertiary screen prioritizing ORFs encoding known membrane trafficking domains (e.g., PH, BAR, ENTH, and PX). Using these criteria, we identified the PX domain–containing *MDM1* as a poorly characterized ORF whose deletion affected Mup1-pH vacuolar sorting. Yeast lacking *MDM1* displayed Mup1-pH accumulation on the vacuole surface (class 3) and cytoplasmic foci (class 2) after methionine (Fig. 1 C). Imaging indicated a lack of a class E dot, observed when vacuolar sorting is blocked (Coonrod and Stevens, 2010), suggesting that *mdm1*Δ yeast partially missorted Mup1-pH. To further confirm that loss of *mdm1* causes defects in endomembrane trafficking, we also conducted bulk endocytic assays using the fluorescent lipid marker FM4-64. Whereas FM4-64 is efficiently endocytosed and delivered to the vacuole surface in wild-type cells, *mdm1*Δ yeast displayed moderate delays in vacuolar delivery and FM4-64 accumulation in endosomal structures (Fig. S1 A). *mdm1*Δ yeast also displayed mild defects in the vacuolar sorting of GFP-Cps1 to the vacuole, suggesting a moderate general defect in endomembrane trafficking (Fig. S1 B). Consistent with this, database searches revealed that the closest human homologue of Mdm1 was regulator of G protein signaling (RGS)–PX1/Snx13, which was previously implicated in general endolysosomal dynamics (Zheng et al., 2006). We thus chose to further characterize Mdm1.

Mdm1 was initially identified as a soluble protein necessary for the inheritance of mitochondria into the yeast bud (McConnell and Yaffe, 1992). However, subsequent whole genome sequencing revealed that *MDM1* was misannotated, initiating at an internal ATG codon approximately two thirds into the ORF (Fig. 1 D). Rather, Mdm1 and its homologues are predicted integral membrane proteins, and TMHMM identifies an N-terminal signal sequence and two transmembrane helices (Krogh et al., 2001). The transmembrane region is followed by a poorly characterized PX-associated (PXA) domain and RGS domain, which was previously identified as a GTPase-activating protein for $G\alpha_s$ subunits in G protein–coupled receptor signaling (Zheng et al., 2001). The Mdm1 C-terminal region contains a PX homology domain, followed by an uncharacterized C-Nexin domain. Notably, this domain architecture is highly conserved from yeast to man with obvious orthologues in all examined metazoans. Humans encode four orthologues: Snx13, 14, 19, and 25 (Fig. 1 D).

Mdm1 is a novel ER–vacuole tethering protein

To determine the subcellular localization of Mdm1, we generated chromosomally tagged *MDM1-GFP* yeast and observed Mdm1-GFP at distinct patches in the cell interior (Fig. 1 E and Table S1). These patches were enriched at the interface between the yeast vacuole and nucleus, both visible by dynamic interference contrast (DIC) microscopy. To confirm this localization, we colabeled *MDM1-GFP* yeast with the vacuole lumenal

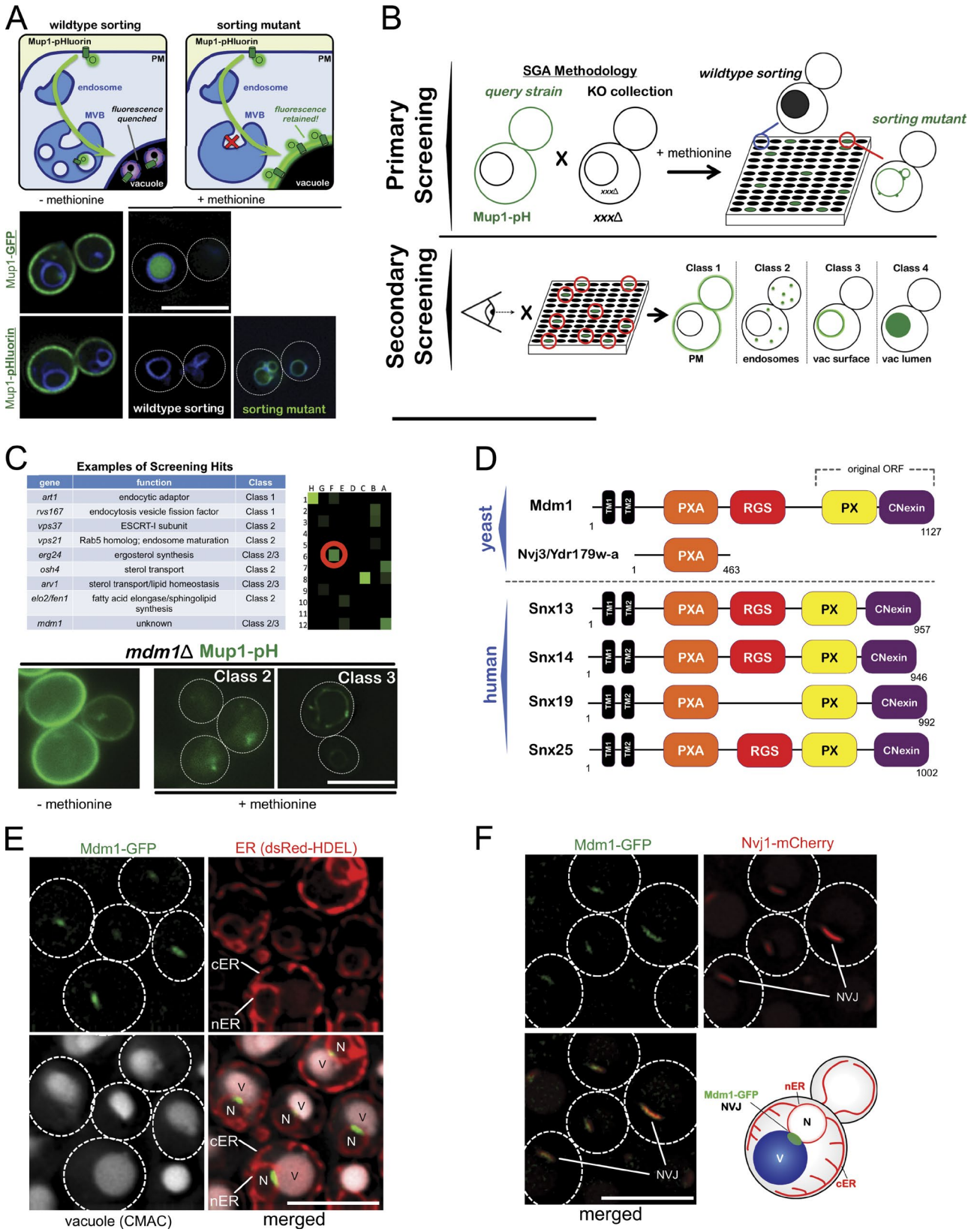

Figure 1. **Mdm1 is a novel interorganelle tether.** (A) Schematic of Mup1-pH trafficking screen. (B) Stages of Mup1-pH screen. (C) Table of several mutants detected in screening. Images are representative *mdm1*Δ Mup1-pH cells displaying class 2/3 sorting defects. (D) Domain architecture of Mdm1/Snx13 family proteins. (E) Yeast expressing Mdm1-GFP and DsRed-HDEL (ER) marker and stained with the vacuole marker CMAC (white). (F) Yeast colabeled with Mdm1-GFP and Nvj1-mCherry. A schematic of Mdm1-GFP at the NVJ. Dotted lines indicate the cell periphery, based on DIC images. MVB, multivesicular body; N, nucleus; V, vacuole. Bars, 5 µm.

marker 7-amino-4-chloromethylcoumarin (CMAC) and the ER marker DsRed-HDEL, which labels both cortical ER and nER. Remarkably, Mdm1-GFP localized to yeast ER–vacuole MCSs, previously denoted as NVJs (Fig. 1 E). Mdm1-GFP colocalized with Nvj1-mCherry, confirming its NVJ localization (Fig. 1 F).

Because Mdm1 appeared to colocalize with a known NVJ resident protein, we next investigated whether the loss of other NVJ proteins would exacerbate the trafficking defects originally observed in *mdm1*Δ yeast. Consistent with this, additional KOs of NVJ resident proteins led to pronounced FM4-64 and GFP-Cps1 trafficking defects, suggesting that loss of these proteins promotes general endomembrane trafficking defects (Fig. S1, A and B).

Because Mdm1 is a predicted transmembrane protein, we hypothesized that it may be topologically anchored in the nER through its N-terminal transmembrane helices and thereby contact the vacuole surface in trans with its C-terminal PX domain, which binds PI3P with high affinity (Yu and Lemmon, 2001). This is supported by previous work showing the vacuolar soluble NSF attachment protein receptor (SNARE) protein Vam7 is recruited to vacuoles through its PI3P-binding PX domain (Cheever et al., 2001).

To test these hypotheses, we generated a truncated Mdm1 construct encoding only the first 389 amino acids (encoding up to the PXA domain) followed by a C-terminal GFP tag (Mdm-1^{1toPXA}-GFP; Table S2). In contrast to full-length (FL) Mdm1, $Mdm1^{1toPXA}$-GFP lost NVJ localization and redistributed across the ER network (Fig. 2, A and B). Linear profile tracing confirmed that $Mdm1^{1toPXA}$-GFP localized to the ER.

To determine whether the Mdm1 PX domain binds the vacuole, we generated a GFP-tagged construct encoding only the Mdm1 PX domain (GFP-$Mdm1^{PX}$). As predicted, GFP-$Mdm1^{PX}$ decorated the vacuole surface (Fig. 2 C). Linear profile tracing confirmed the vacuolar $Mdm1^{PX}$-GFP localization, coinciding with a loss of ER localization.

To confirm that the Mdm1 PX domain binds vacuolar PI3P, we expressed GFP-$Mdm1^{PX}$ in yeast expressing a temperature-sensitive allele of the PI3 kinase Vps34 (*vps34*^{ts}). Whereas growth of this strain at 26°C permitted vacuolar localization of the Mdm1 PX domain, shift to the nonpermissive 37°C temperature induced a loss of PI3P and a redistribution of GFP-$Mdm1^{PX}$ into the cytoplasm (Fig. S1 C). Collectively, these experiments imply that Mdm1 is an ER-anchored integral protein capable of binding the vacuole in trans.

A lipid-binding PX domain is necessary for ER–vacuole Mdm1 tethering

We next tested whether PX-mediated lipid binding was sufficient for Mdm1 vacuole association. PX sequence alignments indicated that the 823-RRY-825 lipid-binding motif is conserved in Mdm1, with R823 residing near the putative lipid-binding pocket of the Snx14 PX domain (Fig. 2 D; Mas et al., 2014). To test whether this lipid-binding pocket is functionally important for the localization of Mdm1, we generated mutant GFP-$Mdm1^{PX\ R823E}$. In contrast to the wild-type PX construct, GFP-$Mdm1^{PX\ R823E}$ failed to decorate the vacuole surface and redistributed into the cytoplasm (Fig. 2 E).

Next, we tested whether the R823E mutation affected FL Mdm1. Strikingly, $Mdm1^{FL\ R823E}$-GFP failed to localize to NVJs, instead redistributing across the ER, suggesting that a lipid-binding PX is necessary for NVJ localization (Fig. 2, F and G).

Mdm1 modulates ER–vacuole tethering

Because Mdm1 appeared to be a previously unrecognized ER–vacuole MCS tether, we next tested whether its expression level could modulate the degree of ER–vacuole tethering. We cloned Mdm1-GFP into a vector under the control of the *glyceraldehyde 3-phosphate* (*GPD*) promoter (P_{GPD}), which up-regulates protein expression ∼20-fold. Remarkably, overexpressed Mdm1-GFP distributed across a hyperelongated vacuole–nER interface (Fig. 3 A). This resulted in drastic vacuole remodeling into tubule- or cup-like structures that surrounded the nER, and quantification revealed an ∼3.9-fold increase in NVJ length (Fig. 3 B). Similar nER–vacuole hypertethering was previously observed after the overexpression of the established NVJ tether Nvj1 (Pan et al., 2000). To confirm that the GFP tag did not contribute to interorganelle tethering, we overexpressed untagged Mdm1 in Nvj1-mCherry yeast. Mdm1 overexpression again induced nER–vacuole hypertethering and an elongation of Nvj1-mCherry–positive NVJs (Fig. S1, D and E).

To better visualize Mdm1-mediated hypertethering, we conducted thin-section transmission EM (TEM). Again, we observed nER–vacuole hypertethering in cells overexpressing Mdm1-GFP (Fig. 3, C and D; NVJs highlighted in yellow). NVJs were characterized by very close (10.5 ± 1 nm) contacts between the nER and vacuole (Fig. 3, E and F). These observations strongly suggest that Mdm1 functions as an nER–vacuole interorganelle tether in yeast.

Nvj3/Ydr179w-a is a second, novel ER–vacuole MCS protein

All Mdm1 homologues encode an uncharacterized PXA domain. Database searches revealed *YDR179W-A* as a second, putative PXA domain–containing ORF in yeast. To determine its localization, we GFP tagged the *YDR179W-A* locus and observed that Ydr179w-a–GFP also localized to NVJs (Fig. 4 A). A tBFP2-tagged Ydr179w-a colocalized with Mdm1-GFP, confirming its NVJ localization, and thus we name it Nvj3 (Fig. S2 A).

Because Nvj3 is predicted to be soluble, we hypothesized that it required Mdm1 for its NVJ localization. Consistent with this, Nvj3-GFP redistributed into the cytoplasm in *mdm1*Δ cells, suggesting Nvj3 interacts directly with Mdm1 at NVJs (Fig. 4 B).

Mdm1 and Nvj3 ER–vacuole MCS localization is independent of Nvj1

Previous studies suggest that an Nvj1–Vac8 interaction is required for ER–vacuole tethering (Kvam and Goldfarb, 2004; Toulmay and Prinz, 2012). To test whether Mdm1 and Nvj3/Ydr179w-a require Nvj1 for their NVJ localization, we examined them in *nvj1*Δ yeast. Remarkably, both Mdm1 and Nvj3 retained ER–vacuole MCS localizations in *nvj1*Δ yeast but were no longer restricted to NVJ patches. Mdm1-GFP retained a punctal distribution, but relocalized to ER tubules and the cortical ER (Fig. 4, C–E). However, each Mdm1-GFP focus was clearly adjacent to the vacuole, suggesting Mdm1 retained vacuole contact at ER–vacuole MCSs in the absence of Nvj1. Linear profiling confirmed maximal Mdm1-GFP focus enrichment at ER and vacuole interfaces (Fig. 4 E). Similarly, Nvj3-GFP also retained ER–vacuole MCS localization in *nvj1*Δ yeast (Fig. 4 F). In some cells, Nvj3 was clearly enriched at the tips of ER tubules making contact with the vacuole, confirming ER–vacuole tethering does not require Nvj1 (Fig. 4, G and H).

Because Mdm1 appeared to localize to ER–vacuole MCSs even in the absence of Nvj1, we also asked the inverse:

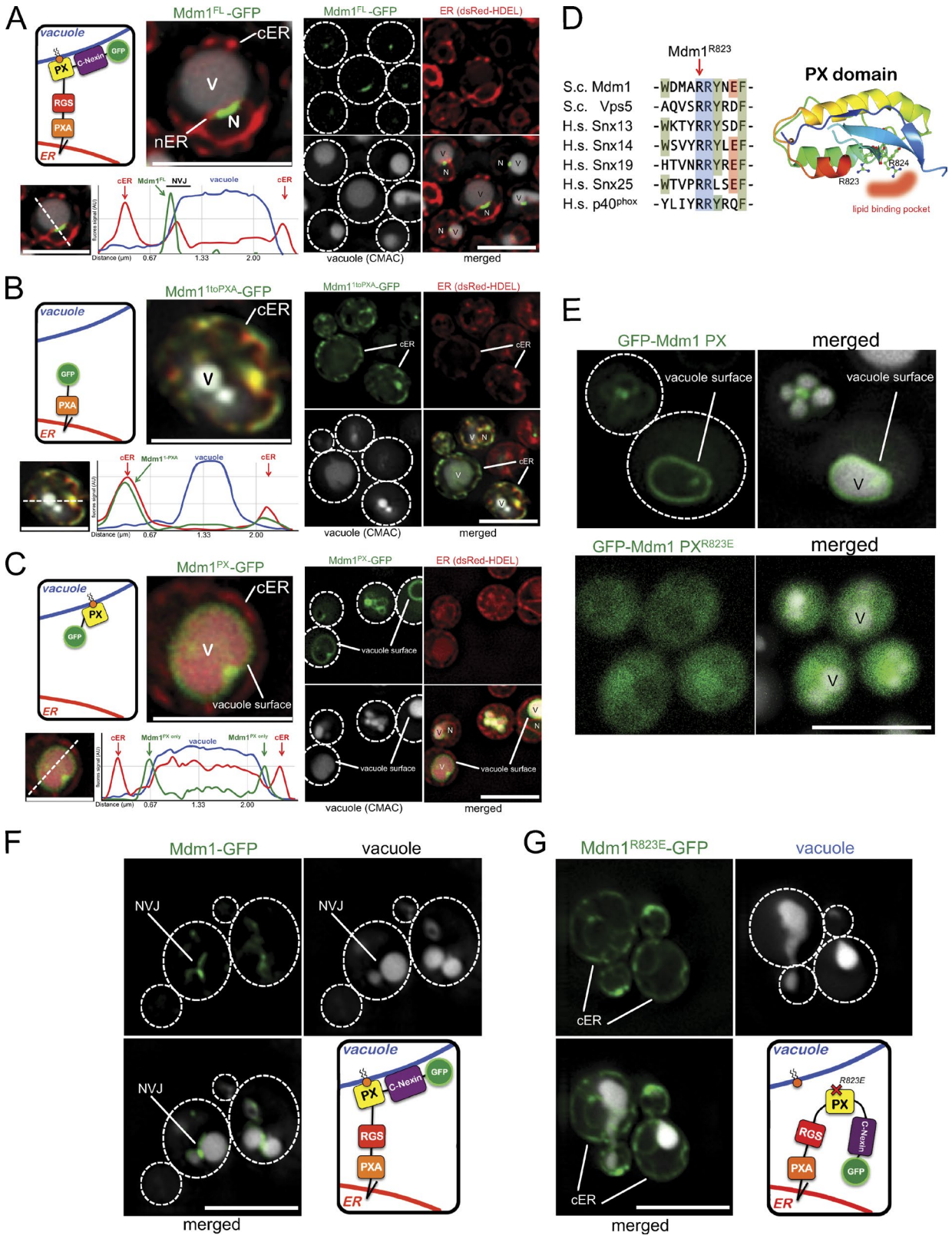

Figure 2. **Mdm1 is anchored in the ER by its transmembrane region and binds in trans to vacuolar PI3P.** (A–C) Yeast colabeled with DsRED-HDEL, CMAC, and either FL Mdm1 (A), Mdm1^{1toPXA}-GFP (B), or the Mdm1 PX domain only (Mdm1^{PX}-GFP; C). A linear profile of the cell shows Mdm1-GFP colocalization relative to the ER and/or vacuole. The linear profiles are profiles from single cells that are highly representative of many cells from at least three independent experiments, where >100 cells were observed to display an Mdm1-GFP distribution like this in each experiment. (D) Alignment of the lipid-binding region of PX domains, with R823 denoted. Structure of the PX domain of Snx14 (Protein Data Bank accession no. 4PQO; Mas et al., 2014). (E) Yeast stained with CMAC and expressing either GFP-Mdm1 PX (top) or the lipid-binding mutant GFP-Mdm1 PX R823E (bottom). (F and G) Yeast stained with CMAC (vacuole) and expressing either wild-type Mdm1 FL–GFP (F) or Mdm1 FL with R823E (G). Dotted lines indicate the cell periphery based on DIC images. AU, arbitrary units; N, nucleus; V, vacuole. Bars, 5 μm.

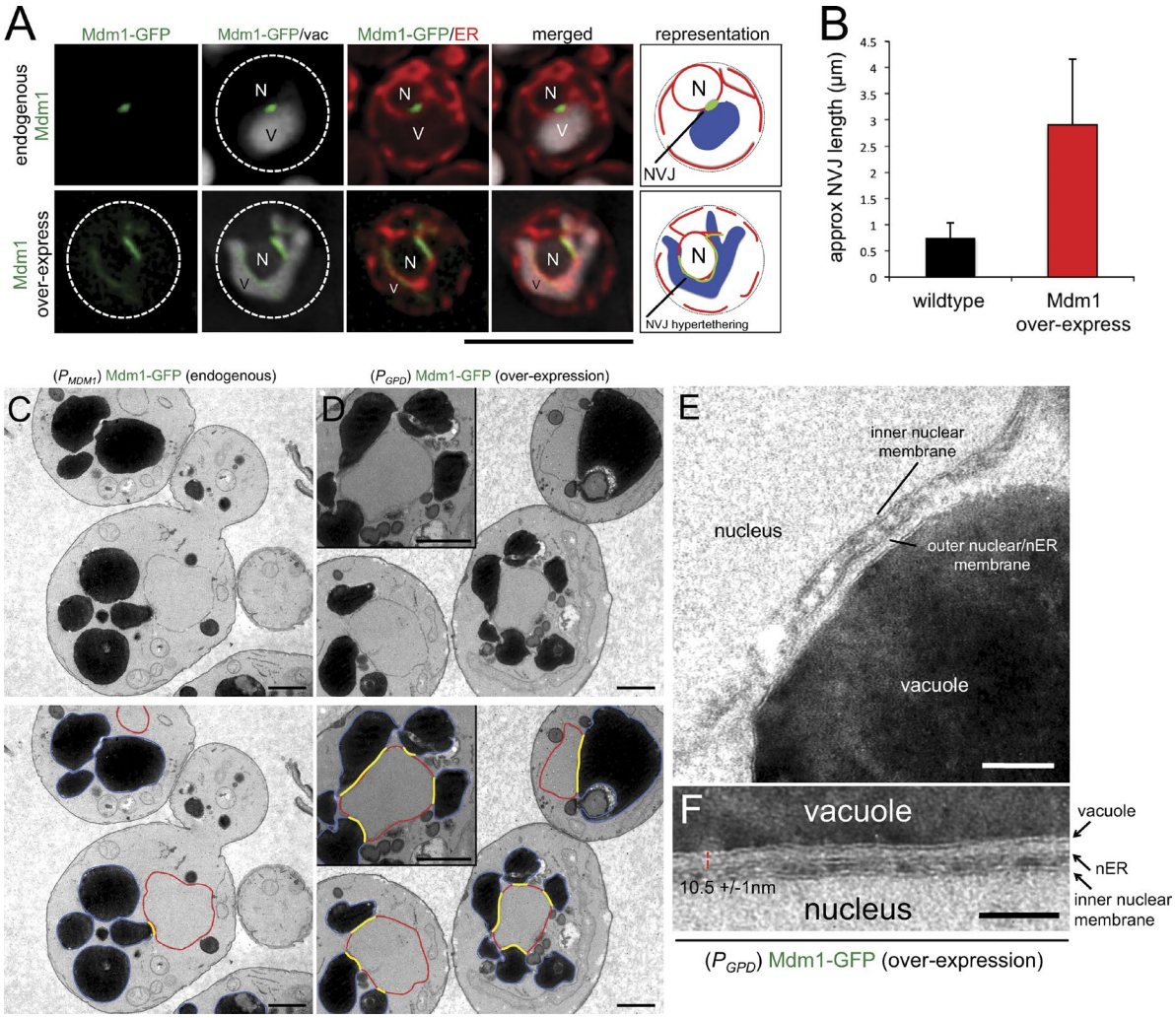

Figure 3. **Overexpression of Mdm1 hypertethers the ER and vacuole.** (A) Yeast stained with CMAC (vacuole; white) and expressing DsRed-HDEL (ER; red) and Mdm1-GFP with either its endogenous promoter (top) or the overexpression GPD promoter (bottom). Bar, 5 µm. (B) Quantitation of NVJ length in >30 cells. Error bars represent the standard error of the measurements. (C and D) Thin-section electron micrographs of yeast endogenously expressing Mdm1 (C) or overexpressing Mdm1 (D). Bottom panels display traces of blue (the vacuole), red (nER), and yellow (NVJs). Bars, 500 nm. (E and F) Magnifications of the NVJs overexpressing Mdm1-GFP. (F) The mean distance between the nER membrane and the vacuole is 10.5 ± 1 nm. N, nucleus; V, vacuole. Bars, 100 nm.

whether loss of Mdm1 affected Nvj1–Vac8-dependent NVJ formation. Indeed, Nvj1 localized to prominent NVJ patches even in *mdm1*Δ yeast, and NVJs appeared normal, suggesting the loss of Mdm1 does not drastically affect Nvj1–Vac8-mediated NVJ formation (Fig. S2 B).

Because ER–vacuole contact continues without Nvj1, we next asked whether these two organelles could be disconnected through the further removal of the ER–vacuole tethering machinery. We generated yeast lacking Mdm1 and Nvj3, as well as quadruple KO yeast lacking Mdm1, Nvj3, Nvj1, and Nvj2 (another NVJ resident protein; Fig. S3, A–C). These strains were viable and displayed no obvious growth defects on nutrient-rich media. In addition, we noted an increase in vacuole size in the quadruple KO (Fig. S3 C). TEM suggested the KO strains had reduced ER–vacuole contact. However, this technique is limited to the 70-nm-thick sections, so is therefore not sufficient to fully image ER–vacuole contacts. Subsequent light microscopy suggested even the quadruple KO yeast display closely juxtaposed nER and vacuoles (Fig. S3 C). However, it should be noted that both the vacuole and nucleus (i.e., nER envelope) are large, so we cannot exclude the possibility that they passively collide even in the absence of tethering machinery.

Mdm1 is consumed by, but is not required for, NVJ-mediated PMN

A few studies have implicated the *Saccharomyces cerevisiae* NVJ in a specific form of microautophagy in which nonessential portions of the nuclear envelope are directly engulfed by the vacuole (PMN; Roberts et al., 2003; Krick et al., 2008). To test whether Mdm1 and Nvj3 also participate in PMN, we first defined a condition that induced PMN by monitoring the incorporation of Nvj1-mCherry into NVJ-derived vesicles that bud into the vacuole lumen. Consistent with previous studies, chronic nitrogen depletion successfully induced PMN, leading to the incorporation of Nvj1-mCherry–positive vesicles into the vacuole (Fig. S2 C). We next asked whether Mdm1 and Nvj3 are required for PMN by monitoring PMN vesicle formation in *mdm1*Δ *nvj3*Δ yeast. Intriguingly, Nvj1-mCherry–positive PMN vesicles formed even in the absence of Mdm1 and Nvj3, suggesting they are not required for yeast PMN (Fig. S2 D).

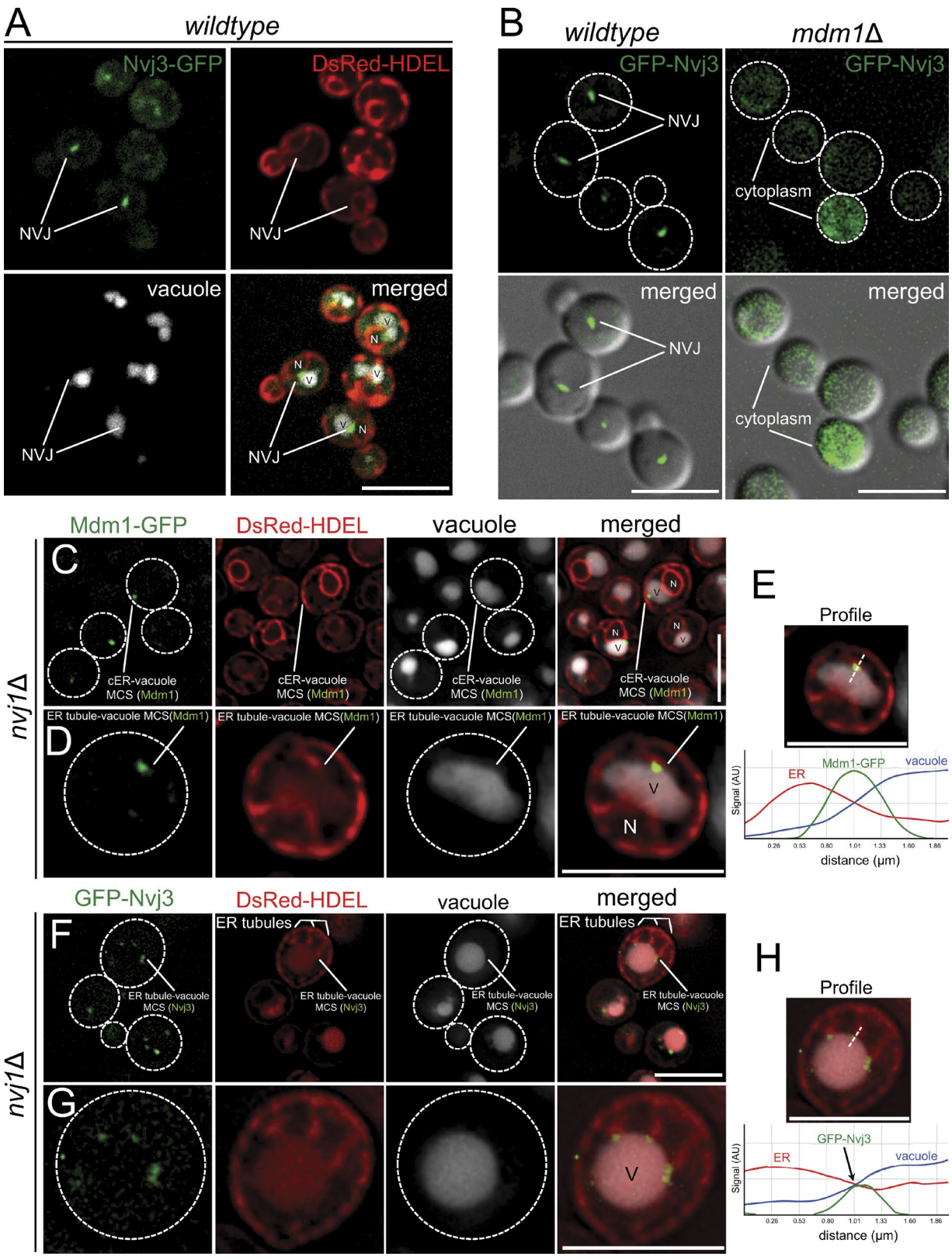

Figure 4. **Mdm1 and Nvj3 localize to the NVJ in an Nvj1-independent manner.** (A) Yeast expressing Nvj3-GFP and DsRed-HDEL (ER), with vacuoles (white). (B) Wild-type and *mdm1*Δ yeast expressing GFP-Nvj3. (C and D) *nvj1*Δ yeast expressing Mdm1-GFP and DsRed-HDEL (ER) and stained with CMAC. (E) Linear profile of Mdm1-GFP–positive NVJ in *nvj1*Δ yeast. (F and G) *nvj1*Δ yeast expressing GFP-Nvj3, DsRed-HDEL (ER), and vacuoles (white). (H) Linear profile of a GFP-Nvj3–positive NVJ in *nvj1*Δ yeast. The linear profiles in E and H are from single cells that are highly representative of many cells from at least three independent experiments. White dotted lines denote the cell periphery. AU, arbitrary units; N, nucleus; V, vacuole. Bars, 5 μm.

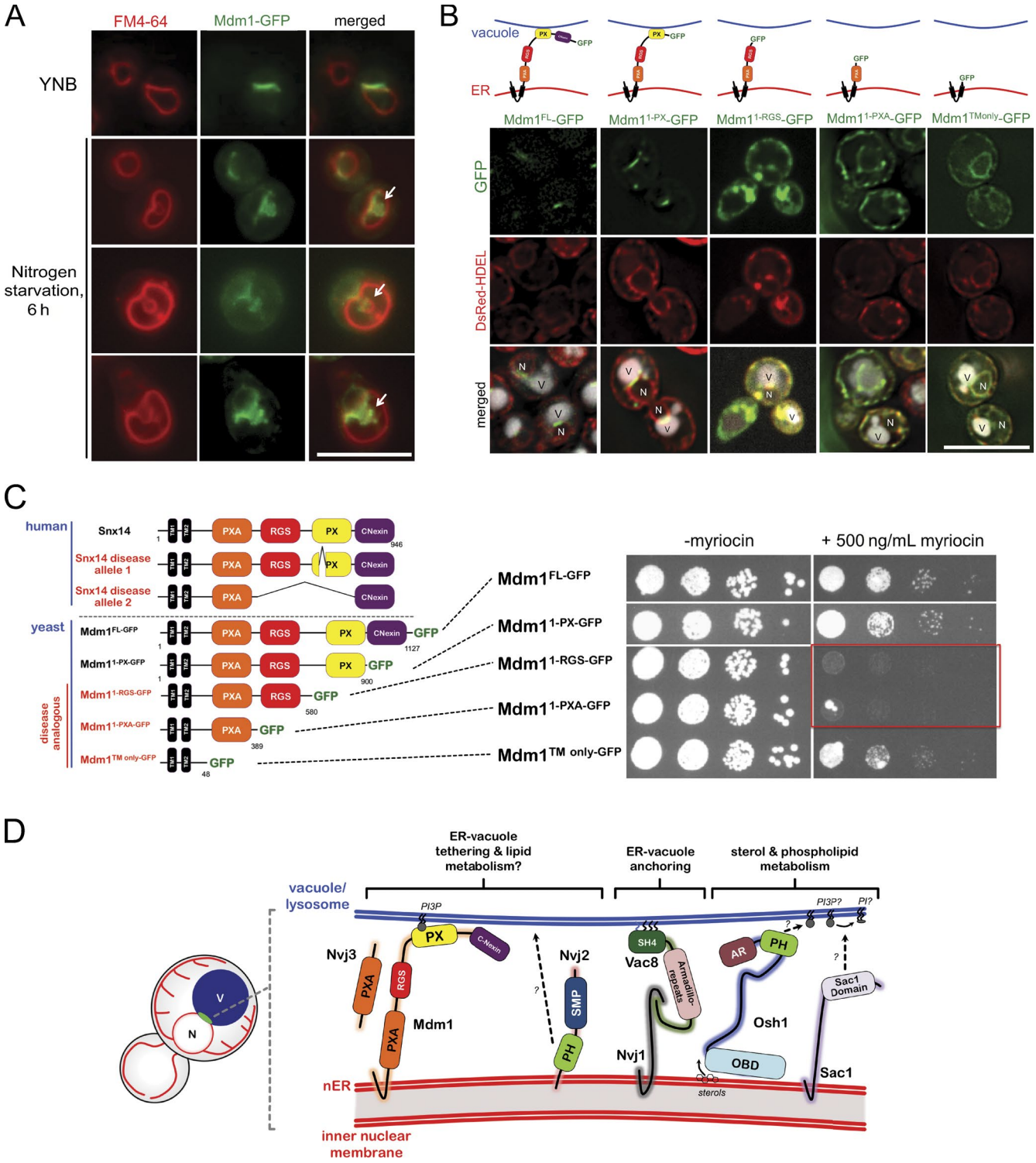

Figure 5. ***SNX14* disease-analogous Mdm1 alleles perturb yeast sphingolipid metabolism.** (A) Yeast with labeled vacuoles (FM4-64) under nitrogen starvation undergo PMN that consumes Mdm1-GFP. Arrows show PMN invaginations. (B) Yeast expressing a series of Mdm1-GFP truncations, DsRed-HDEL, and CMAC (white; vacuole). (C, left) Domain architecture of human Snx14 and its disease-associated alleles compared with Mdm1 truncations. (right) Correlative plating assay of yeast overexpressing Mdm1 truncations on media ± 500 ng/ml myriocin. The red box indicates RGS. (D) Model for the yeast NVJ showing novel proteins Nvj3 and Mdm1. Question marks denote hypothetical interactions. AR, armadillo repeats; N, nucleus; OBD, oxysterol binding domain; PH, pleckstrin homology; SMP, synaptotagmin-like mitochondrial lipid-binding protein domain; V, vacuole. Bars, 5 µm.

Finally, we investigated whether Mdm1 is a substrate for PMN by monitoring its localization during nitrogen starvation. Strikingly, Mdm1-GFP was efficiently incorporated into prominent FM4-64–positive invaginations that protruded into the vacuole interior, indicating Mdm1 is consumed like Nvj1 during PMN (Fig. 5 A). Collectively, these observations indicate that Mdm1 is acutely localized to the NVJ and selectively consumed by PMN during nitrogen starvation.

Snx14 disease-associated mutations in Mdm1 lose MCS localization and perturb sphingolipid metabolism

Mutations in Mdm1 homologue Snx14 were recently associated with a neurological disease characterized by cerebellar ataxia, intellectual disability, cellular vacuolization, and the accumulation of granular deposits in the cytoplasm of patients' fibroblasts (Thomas et al., 2014; Akizu et al., 2015). All disease-associated alleles carry deletions affecting the PX domain, suggesting loss of PX lipid binding may contribute to pathology. To begin to understand Mdm1/Snx14 proteins in disease, we generated GFP-tagged Mdm1 truncations that mimicked the loss of the PX domain and determined their localization (Fig. 5 B). Both the $Mdm1^{FL}$-GFP and an Mdm1 truncation lacking the C-terminal C-Nexin domain ($Mdm1^{1\text{-}PX}$-GFP) localized to NVJs, indicating the C-Nexin domain is dispensable for ER–vacuole tethering (Fig. 5 B). In contrast, truncations removing the PX domain ($Mdm1^{1\text{-}RGS}$-GFP, $Mdm1^{1\text{-}PXA}$-GFP, and $Mdm1^{TMonly}$-GFP) lost NVJ localization and redistributed across the ER (Fig. 5 B). An Mdm1 allele carrying a deletion within the PX domain ($Mdm1^{\Delta 813–841}$GFP) directly analogous to the disease-associated $Snx14^{\Delta 603–632}$ allele also distributed across the ER, again indicating the PX domain is necessary for ER–vacuole tethering (Fig. S2 E).

MCSs are proposed sites of lipid metabolism and interorganelle lipid exchange (Elbaz and Schuldiner, 2011; Toulmay and Prinz, 2012). NVJs in particular are sites of long chain fatty acid synthesis, a component of the sphingolipid biosynthetic pathway (Kvam et al., 2005). Numerous neurological diseases (Niemann-Pick types A and B, Fabry's, Tay-Sachs, and Gaucher's) are characterized by cellular vacuolization and the pathological accumulation of sphingolipids in intracellular granular-like deposits (Kivalo and Stjernvall, 1958; Brady et al., 1967). To determine whether the disease-associated Mdm1 truncations affect sphingolipid metabolism in yeast, we grew yeast overexpressing each Mdm1 truncation on media containing the sphingolipid synthesis inhibitor myriocin. Strikingly, overexpression of these nontethering disease-analogous Mdm1 alleles induced hypersensitivity to myriocin, suggesting they perturb sphingolipid biosynthesis (Fig. 5 C and Fig. S2 E). This was not simply caused by the overexpression of an ER-anchored membrane protein, as overexpression of a nontethering Nvj1 mutant ($Nvj1^{1–144}$GFP) failed to induce myriocin sensitivity (Fig. S2 E). Intriguingly, further truncation of Mdm1 that removed the PXA domain suppressed this growth defect, implying the PXA domain is necessary for myriocin sensitivity. Expression of a soluble PXA domain lacking the transmembrane region was also not sensitive to myriocin, indicating that an ER-localized PXA is required to sensitize yeast to myriocin (Fig. S2 F). This myriocin sensitivity was also Nvj3 independent (Fig. S2 G).

Collectively, these observations suggest Mdm1 and Nvj3 are novel NVJ proteins. Contrary to previous studies (Pan et al., 2000; Kvam et al., 2005), we propose that ER–vacuole tethering occurs in the absence of Nvj1 (Fig. 4, C–G). As Nvj1 and Vac8 have no clear homologues in metazoans, Mdm1 family proteins may constitute the first ER–endolysosomal tethers with clear homologues from yeast to man. Given that interorganelle MCSs are implicated in lipid homeostasis, we speculate that the disease-associated Snx14 alleles may perturb ER–endolysosomal interorganelle communication and may additionally perturb aspects of lipid and/or sphingolipid metabolism, contributing to neurological disease. In yeast, the PXA domain is the only domain shared between Mdm1 and Nvj3 and is unique to these proteins, making it specifically localized to ER–vacuole MCSs. This, combined with the observation that an ER-anchored PXA domain is sufficient to induce myriocin hypersensitivity when overexpressed, suggests PXA domains may play a direct role in lipid metabolism through interacting with lipids or ER metabolic proteins. Further studies are needed to reveal the functions of PXA domain–containing proteins in interorganelle communication and lipid metabolism.

Materials and methods

Molecular biology, yeast genetics, and cloning

Yeast genetic manipulations were conducted using classical yeast knock-in/out protocols. For ectopic protein expression, genes were cloned into pBP73-C or -G vectors encoding either the GPD promoter or carboxypeptidase Y (CPY) promoter using XbaI–XhoI MCSs. All constructs were sequenced. PX domain alignment was generated using CLUSTALW (Conway Institute, University College Dublin).

SGA methodology and Mup1-pHuorin screening

To make the Mup1-pH KO library, a MATα *MUP1-PHLUORIN::clonNAT* query strain was generated from Y8205 yeast (a gift from C. Boone, University of Toronto, Toronto, Ontario, Canada). The query strain was mated to the MATa nonessential KO collection grown in 384-well format using an automation workstation (BioMek NX; Beckman Coulter). Diploids were grown and sporulated, and desired haploids were selected on plates. Screening was conducted on a flow cytometer (Accuri C6; BD).

Light microscopy

Living yeast were cultured in yeast extract peptone dextrose or yeast nitrogen base selective growth media and grown to an OD_{600} of ∼0.8 before imaging. The vacuole lumenal dye CMAC or FM4-64 (Life Technologies) was added for 10 min, and then yeast were pelleted, washed, and imaged. For nitrogen starvation PMN experiments, yeast were cultured in nitrogen-rich (0.67% nitrogen base) or low-nitrogen (0.17% nitrogen base) selective media for 6 h at room temperature. Living yeast were mostly imaged using a DeltaVision RT system (Applied Precision) equipped with a microscope (IX71; Olympus), a camera (CoolSNAP HQ; Photometrics), and DeltaVision RT software. All yeast were imaged at 26°C in yeast nitrogen base medium unless otherwise noted. Images were acquired with a 63× (1.40 NA) objective. A few images were acquired using a cell imaging system (EVOS FL; Life Technologies) equipped with a 100× Plan Fluorite (1.28 NA; Life Technologies) objective and a monochrome CCD camera (ICX445; Sony). All line profiles and analysis were conducted using ImageJ (National Institutes of Health)/Fiji.

EM

Yeast were fixed with 2.5% (vol/vol) glutaraldehyde for 1 h and incubated in 1% potassium permanganate for 1 h. Cells were dehydrated with 50, 70, 95, and 100% ethanol. Samples were transitioned into 100% propylene oxide, embedded in Spurr's resin, and sectioned with a serial microtome. EM was performed using a transmission electron microscope (Morgnani 268; FEI) with a digital camera (Advanced Microscopy Techniques, Corp.) and an 80-keV beam.

Yeast myriocin plating assays

Yeast were grown in yeast nitrogen base–Ura selective media to an OD_{600} of ∼0.8, and then 10× dilutions were made in 96-well

plates and replica were pinned on 500 ng/ml myriocin plates. Cells were imaged at 4 d of growth.

Online supplemental material

Fig. S1 shows experiments detailing the trafficking defects associated with loss of Mdm1, as well as how the Mdm1 PX domain binds to PI3P and its overexpression induces ER–vacuole hypertethering. Fig. S2 shows experiments implicating Mdm1 in PMN and the effects of Mdm1 PXA domain overexpression on sphingolipid metabolism. Fig. S3 shows TEM micrographs of wild-type, *mdm1*Δ*nvj3*Δ, and *mdm1*Δ*nvj3*Δ*nvj1*Δ*nvj2*Δ yeast. Table S1 shows all strains used in this study. Table S2 shows all plasmids used in this study. Online supplemental material is available at http://www.jcb.org/cgi/content/full/jcb.201503088/DC1.

Acknowledgments

The authors would like to thank Tony Gatts IV for his technical expertise in TEM. We also thank Hansen Xu, Ming Li, Joel Goodman, Jennifer Liou, and members of the Emr laboratory for helpful discussions.

W.M. Henne is supported by a Welch Foundation grant (I-1873). S.D. Emr is supported by a Cornell University grant.

The authors declare no competing financial interests.

Submitted: 19 March 2015
Accepted: 14 July 2015

References

Akizu, N., V. Cantagrel, M.S. Zaki, L. Al-Gazali, X. Wang, R.O. Rosti, E. Dikoglu, A.B. Gelot, B. Rosti, K.K. Vaux, et al. 2015. Biallelic mutations in *SNX14* cause a syndromic form of cerebellar atrophy and lysosome-autophagosome dysfunction. *Nat. Genet.* 47:528–534. http://dx.doi.org/10.1038/ng.3256

Alpy, F., A. Rousseau, Y. Schwab, F. Legueux, I. Stoll, C. Wendling, C. Spiegelhalter, P. Kessler, C. Mathelin, M.C. Rio, et al. 2013. STARD3 or STARD3NL and VAP form a novel molecular tether between late endosomes and the ER. *J. Cell Sci.* 126:5500–5512. http://dx.doi.org/10.1242/jcs.139295

Beh, C.T., and J. Rine. 2004. A role for yeast oxysterol-binding protein homologs in endocytosis and in the maintenance of intracellular sterol-lipid distribution. *J. Cell Sci.* 117:2983–2996. http://dx.doi.org/10.1242/jcs.01157

Brady, R.O., A.E. Gal, R.M. Bradley, E. Martensson, A.L. Warshaw, and L. Laster. 1967. Enzymatic defect in Fabry's disease—Ceramidetrihexosidase deficiency. *N. Engl. J. Med.* 276:1163–1167. http://dx.doi.org/10.1056/NEJM196705252762101

Buchkovich, N.J., W.M. Henne, S. Tang, and S.D. Emr. 2013. Essential N-terminal insertion motif anchors the ESCRT-III filament during MVB vesicle formation. *Dev. Cell.* 27:201–214. http://dx.doi.org/10.1016/j.devcel.2013.09.009

Cheever, M.L., T.K. Sato, T. de Beer, T.G. Kutateladze, S.D. Emr, and M. Overduin. 2001. Phox domain interaction with PtdIns(3)P targets the Vam7 t-SNARE to vacuole membranes. *Nat. Cell Biol.* 3:613–618. http://dx.doi.org/10.1038/35083000

Coonrod, E.M., and T.H. Stevens. 2010. The yeast vps class E mutants: the beginning of the molecular genetic analysis of multivesicular body biogenesis. *Mol. Biol. Cell.* 21:4057–4060. http://dx.doi.org/10.1091/mbc.E09-07-0603

Costanzo, M., and C. Boone. 2009. SGAM: an array-based approach for high-resolution genetic mapping in *Saccharomyces cerevisiae*. *Methods Mol. Biol.* 548:37–53. http://dx.doi.org/10.1007/978-1-59745-540-4_3

Eden, E.R., I.J. White, A. Tsapara, and C.E. Futter. 2010. Membrane contacts between endosomes and ER provide sites for PTP1B–epidermal growth factor receptor interaction. *Nat. Cell Biol.* 12:267–272.

Elbaz, Y., and M. Schuldiner. 2011. Staying in touch: the molecular era of organelle contact sites. *Trends Biochem. Sci.* 36:616–623. http://dx.doi.org/10.1016/j.tibs.2011.08.004

Elbaz-Alon, Y., E. Rosenfeld-Gur, V. Shinder, A.H. Futerman, T. Geiger, and M. Schuldiner. 2014. A dynamic interface between vacuoles and mitochondria in yeast. *Dev. Cell.* 30:95–102. http://dx.doi.org/10.1016/j.devcel.2014.06.007

Friedman, J.R., J.R. Dibenedetto, M. West, A.A. Rowland, and G.K. Voeltz. 2013. Endoplasmic reticulum–endosome contact increases as endosomes traffic and mature. *Mol. Biol. Cell.* 24:1030–1040. http://dx.doi.org/10.1091/mbc.E12-10-0733

Guan, X.L., C.M. Souza, H. Pichler, G. Dewhurst, O. Schaad, K. Kajiwara, H. Wakabayashi, T. Ivanova, G.A. Castillon, M. Piccolis, et al. 2009. Functional interactions between sphingolipids and sterols in biological membranes regulating cell physiology. *Mol. Biol. Cell.* 20:2083–2095. http://dx.doi.org/10.1091/mbc.E08-11-1126

Henne, W.M., N.J. Buchkovich, Y. Zhao, and S.D. Emr. 2012. The endosomal sorting complex ESCRT-II mediates the assembly and architecture of ESCRT-III helices. *Cell.* 151:356–371. http://dx.doi.org/10.1016/j.cell.2012.08.039

Hönscher, C., M. Mari, K. Auffarth, M. Bohnert, J. Griffith, W. Geerts, M. van der Laan, M. Cabrera, F. Reggiori, and C. Ungermann. 2014. Cellular metabolism regulates contact sites between vacuoles and mitochondria. *Dev. Cell.* 30:86–94.

Kivalo, E., and L. Stjernvall. 1958. Vacuolized lymphocytes in juvenile amaurotic idiocy; an electron microscopic study. *Ann. Paediatr. Fenn.* 4:25–29.

Krick, R., Y. Muehe, T. Prick, S. Bremer, P. Schlotterhose, E.L. Eskelinen, J. Millen, D.S. Goldfarb, and M. Thumm. 2008. Piecemeal microautophagy of the nucleus requires the core macroautophagy genes. *Mol. Biol. Cell.* 19:4492–4505. http://dx.doi.org/10.1091/mbc.E08-04-0363

Krogh, A., B. Larsson, G. von Heijne, and E.L. Sonnhammer. 2001. Predicting transmembrane protein topology with a hidden Markov model: application to complete genomes. *J. Mol. Biol.* 305:567–580. http://dx.doi.org/10.1006/jmbi.2000.4315

Kvam, E., and D.S. Goldfarb. 2004. Nvj1p is the outer-nuclear-membrane receptor for oxysterol-binding protein homolog Osh1p in *Saccharomyces cerevisiae*. *J. Cell Sci.* 117:4959–4968. http://dx.doi.org/10.1242/jcs.01372

Kvam, E., K. Gable, T.M. Dunn, and D.S. Goldfarb. 2005. Targeting of Tsc13p to nucleus–vacuole junctions: a role for very-long-chain fatty acids in the biogenesis of microautophagic vesicles. *Mol. Biol. Cell.* 16:3987–3998. http://dx.doi.org/10.1091/mbc.E05-04-0290

Lin, C.H., J.A. MacGurn, T. Chu, C.J. Stefan, and S.D. Emr. 2008. Arrestin-related ubiquitin-ligase adaptors regulate endocytosis and protein turnover at the cell surface. *Cell.* 135:714–725. http://dx.doi.org/10.1016/j.cell.2008.09.025

Mas, C., S.J. Norwood, A. Bugarcic, G. Kinna, N. Leneva, O. Kovtun, R. Ghai, L.E. Ona Yanez, J.L. Davis, R.D. Teasdale, and B.M. Collins. 2014. Structural basis for different phosphoinositide specificities of the PX domains of sorting nexins regulating G-protein signaling. *J. Biol. Chem.* 289:28554–28568. http://dx.doi.org/10.1074/jbc.M114.595959

McConnell, S.J., and M.P. Yaffe. 1992. Nuclear and mitochondrial inheritance in yeast depends on novel cytoplasmic structures defined by the MDM1 protein. *J. Cell Biol.* 118:385–395. http://dx.doi.org/10.1083/jcb.118.2.385

Munn, A.L., A. Heese-Peck, B.J. Stevenson, H. Pichler, and H. Riezman. 1999. Specific sterols required for the internalization step of endocytosis in yeast. *Mol. Biol. Cell.* 10:3943–3957. http://dx.doi.org/10.1091/mbc.10.11.3943

Pan, X., P. Roberts, Y. Chen, E. Kvam, N. Shulga, K. Huang, S. Lemmon, and D.S. Goldfarb. 2000. Nucleus–vacuole junctions in *Saccharomyces cerevisiae* are formed through the direct interaction of Vac8p with Nvj1p. *Mol. Biol. Cell.* 11:2445–2457. http://dx.doi.org/10.1091/mbc.11.7.2445

Pichler, H., and H. Riezman. 2004. Where sterols are required for endocytosis. *Biochim. Biophys. Acta.* 1666:51–61. http://dx.doi.org/10.1016/j.bbamem.2004.05.011

Prosser, D.C., K. Whitworth, and B. Wendland. 2010. Quantitative analysis of endocytosis with cytoplasmic pHluorin chimeras. *Traffic.* 11:1141–1150. http://dx.doi.org/10.1111/j.1600-0854.2010.01088.x

Roberts, P., S. Moshitch-Moshkovitz, E. Kvam, E. O'Toole, M. Winey, and D.S. Goldfarb. 2003. Piecemeal microautophagy of nucleus in *Saccharomyces cerevisiae*. *Mol. Biol. Cell.* 14:129–141. http://dx.doi.org/10.1091/mbc.E02-08-0483

Rowland, A.A., P.J. Chitwood, M.J. Phillips, and G.K. Voeltz. 2014. ER contact sites define the position and timing of endosome fission. *Cell.* 159:1027–1041. http://dx.doi.org/10.1016/j.cell.2014.10.023

Thomas, A.C., H. Williams, N. Setó-Salvia, C. Bacchelli, D. Jenkins, M. O'Sullivan, K. Mengrelis, M. Ishida, L. Ocaka, E. Chanudet, et al. 2014. Mutations in *SNX14* cause a distinctive autosomal-recessive cer-

ebellar ataxia and intellectual disability syndrome. *Am. J. Hum. Genet.* 95:611–621. http://dx.doi.org/10.1016/j.ajhg.2014.10.007

Toulmay, A., and W.A. Prinz. 2012. A conserved membrane-binding domain targets proteins to organelle contact sites. *J. Cell Sci.* 125:49–58. http://dx.doi.org/10.1242/jcs.085118

Yu, J.W., and M.A. Lemmon. 2001. All phox homology (PX) domains from *Saccharomyces cerevisiae* specifically recognize phosphatidylinositol 3-phosphate. *J. Biol. Chem.* 276:44179–44184. http://dx.doi.org/10.1074/jbc.M108811200

Zheng, B., Y.C. Ma, R.S. Ostrom, C. Lavoie, G.N. Gill, P.A. Insel, X.Y. Huang, and M.G. Farquhar. 2001. RGS-PX1, a GAP for $G\alpha_S$ and sorting nexin in vesicular trafficking. *Science.* 294:1939–1942. http://dx.doi.org/10.1126/science.1064757

Zheng, B., T. Tang, N. Tang, K. Kudlicka, K. Ohtsubo, P. Ma, J.D. Marth, M.G. Farquhar, and E. Lehtonen. 2006. Essential role of RGS-PX1/sorting nexin 13 in mouse development and regulation of endocytosis dynamics. *Proc. Natl. Acad. Sci. USA.* 103:16776–16781. http://dx.doi.org/10.1073/pnas.0607974103